EUROPEAN JOURNAL OF COMPUTATIONAL MECHANICS, 2016
VOL. 25, NO. 5, 388–416
http://dx.doi.org/10.1080/17797179.2016.1245597

Taylor & Francis
Taylor & Francis Group

An engineering application of the h-p version of the finite elements method to the dynamics analysis of a symmetrical on-board rotor

Ahmed Saimi and Abdelhamid Hadjoui

IS2M Laboratory, Faculty of Technology, University of Tlemcen, Tlemcen, Algeria

ABSTRACT

The h-p hybrid finite element method is used in this paper for the dynamic analysis of a symmetrical on-board rotor on mobile dimensionally stable supports. The disc and the bearings are assumed to be rigid, with deformable shaft, the material is isotropic. A three-dimensional beam element is used for the discretization of the rotor. In the standard h-version of the finite element, the used shape functions are cubic Hermit, which respect the boundary conditions in all directions, the shape functions-h are modified so they can make the combination between K-orthogonal polynomial shape functions facilitating combination to use the h-p version of the finite element method. Energy method is used for the determination of energy for the entire rotor system. The equations of motion of the rotor system are determined by the Lagrange method. The calculation steps for linear dynamic behaviour of on-board rotor system analysis are grouped in an application created using MATLAB programming language and validated with the work done previously by the classic version of the finite element method. In this paper, we make a comparison of the natural frequencies of on-board rotor system, obtained by the h-p version of the finite element method with version h.

ARTICLE HISTORY
Received 31 May 2016
Accepted 4 October 2016

KEYWORDS
Symmetrical rotor; h-p version of FEM; on-board rotor; rotor dynamics; base excitation

1. Introduction

The h-p version is a general version of the finite element method, a numerical method to solve partial differential equations based on approximations polynomial elements that use variable sized elements (h) and polynomial of degree (p). The origins date back to h-p-MEF innovative work of Babuska and Guo (1992) who discovered that the finite element method converges exponentially fast when the mesh is refined using an appropriate combination of refinements – h (dividing into smaller elements) and – p refinement (by increasing the polynomial degree).

CONTACT Ahmed Saimi ahmedsaimi@hotmail.fr

The exponential convergence makes the method a very attractive choice compared to most other methods of finite elements that converge at an algebraic rate. The exponential convergence of the h-p-MEF was not only theoretically predicted, but observed by many independent researchers.

Many scientists have focused on this axis and have given several finite element codes such as Probe (Szabo, 1985a) and Fiesta (Szabo, 1985b); Heuveline and Rannacher (2003) also worked on the h-p version of the finite element methods, Babuška and Suri (1987) used the h-p version of the finite element method for shells, as there is a study on a beam by the Bernoulli h-p version of the finite element by Bardell (1996), on the other hand in the dynamic field of rotor not many articles by h-p version of the MEF are found, we can cite the work of Boukhalfa and Hadjoui (2010) on composite rotor.

Rotating machines play a vital role in many modern industrial applications. Most of them can be considered as embedded machine mainly affected by an imbalance and excitations due to the support.

Knowledge of the vibration behaviour of the rotors has a great importance for manufacturers and uses of these equipment; many researchers focused their research on this axis and the dynamic behaviour study, especially for critical rotor speeds that differs from its non-rotary natural frequency. The main reason for this difference is known as the gyroscopic effect. Green (1948) for the first time has studied the gyroscopic effect on the normal frequency of flexible rotors. Eshienman and Eubanks (1967) and Rao (1983) also studied the gyroscopic effect on the normal frequency of rotating shafts The external loading can also change the lateral normal frequency of rotating shafts. The effect of the axial force and torque twist externally applied to the lateral vibration of the rotating shafts has been studied by several investigators. Bokaian (1948) introduced the changes in lateral normal frequency of Euler Bernoulli beams under axial load with various boundary conditions. Choi II, Pierre and Ulsoy (1995) derived the equation of a rotating shaft subjected to constant compressive axial load by introducing gyroscopic times. Khader (1995) studied the stability of a cantilever bend shaft with a hard disc at its free end, subjected to axial load and torque. Chen and Sheu (1998) have investigated analytically the behaviour stability of a Timoshenko rotating shaft with a disc subjected to a longitudinal force. They gave the expressions of equations frequencies for different boundary conditions. Chen and Ku (1992) examined the dynamic stability of a cantilever shaft-disc system subject to periodic axial force by the finite element method and have given the limitations of dynamic instability. The inertial forces may also induce axial loads on rotating shafts, and the rotation of a beam around an axis perpendicular to the axis, create centrifugal forces directly producing axial forces in the beam, this phenomenon was also studied by researchers. Banerjee (2000) used the dynamic stiffness matrix for the case of beam of Euler Bernoulli with the axial force for the vibration analysis. Lin and Hsiao (2001) have derived the equation governing linear vibrations of a Timoshenko beam, and proposed a method based on the resolution of the entire

series to reach the final solution which is the natural frequency of the Timoshenko beam. Nelson et al. (1976) used the finite element method to study the rotors on deformable supports. The dynamic behaviour study of a rotor in the boarding effect is the study of the global behaviour of the rotor whose support is subject to any movements. This model is well suited to understand the movement of rotors phenomenon embedded in vehicles, aircraft etc. This phenomenon recently attracted the attention of researchers. Duchemin, Berlioz, and Ferraris (2006) made a detailed study based on the simple model of Rayleigh-Ritz, a rotor whose support is in motion. Various analytical studies were performed on simple movements, simple translation, sinusoidal translation, constant rotation, accelerated rotation. Dakel (2013) continued the work by adding the hydrodynamic bearings by the conventional finite element method. In the work of Boukhalfa and Hadjoui (2010), we find a study on behaviour of composite rotor materials by h-p version finite element. Based on the latter two works, in our case we will make a study of an on-board rotor, whose support is assumed to be rigid and mobile, with the application of the h p-version finite element.

2. Model of on-board rotor

In general, a rotor system is composed of a shaft supported by bearings, and having one or more discs. In this study, the solicitations considered are the imposed displacements of rigid base. The number of each component can be more than one, however, in this paper, the studied rotor has one shaft (single shaft), (see Figure 1)

The assumptions that we consider in this paper are:

- The shaft is deformable and modelled by homogeneous straight beams, isotropic, linear elastic with constants sections subjected to bending moment in two orthogonal directions (horizontal and vertical directions).
- The discs are assumed to be rigid.
- The bearings are assumed to be rigid.
- The rotor support is infinitely rigid; but mobile.

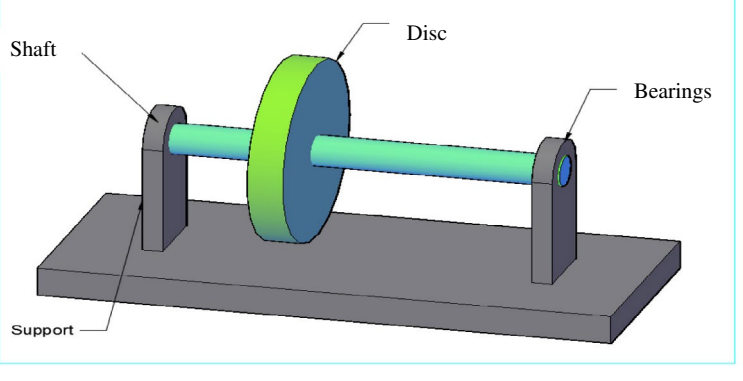

Figure 1. On-board rotor.

The consideration of the motion of the support can significantly affect the form of the equations of motion of a rotor in flexion with respect to those obtained in the case of a fixed support. To obtain the simplest possible model, the approach presented by Duchemin et al. (2006) is used. It offers the modelling of a rotor with mobile support by considering the motion of the rotor relative to the support and that of the support relative to the ground. This is to study the transverse deflections of the mid-line of the rotor shaft relative to a reference linked to the rigid support.

The steps for obtaining the equations of motion are inspired by the approach used by Lalanne and Ferraris (1998), so it needs the description of the movement of the on-board rotor and vectors expressing rotations between them.

The differential equations of the bending motion of an on-board steady rotor are deducted from the equations LAGRANGE applied with respect to the generalised coordinates as follows:

$$\frac{\mathrm{d}}{\mathrm{d}t}\left(\frac{\partial E}{\partial \dot{q}_i}\right) - \frac{\partial E}{\partial q_i} + \frac{\partial U}{\partial q_i} = \delta F_i \tag{1.1}$$

2.1. Equations elaboration

In order not to neglect motion of the support, three main frames are defined:

- The fixed Galilean reference frame $R_g(x_g, y_g, z_g)$
- The reference related to the deformable support $R_s(x_s, y_s, z_s)$,
- The current rotating reference frame, connected to the rotor $R(x, y, z)$.

The centres of these frames are, respectively, O, A and C.

The calculation of the expressions of kinetic energies of the shaft and the disc, requires the calculation of velocity vectors and rotation of the frame R relative to the frame R_g.

Since there are three frames considered, two reference system changes may be performed by:

- Transforming the frame attached to the support R_s to the local frame R
- The transformation of the Galilean reference frame R_g to the frame attached to the support R_s

Generally in rotor dynamics, the rotation of a reference frame R linked to a point in the deformable shaft relative to the frame R_s attached to the support is defined by Euler angles θ_x, $\theta_y et\ \theta_z$ (Figure 2), by involving two intermediate frames.

- A rotation angle θ_z around z_s (intermediate frame $R1(x1, y1, z1)$).
- A rotation angle θ_x around the new axis $x1$ intermediate frame $R2(x2, y2, z2)$).
- A rotation angle θ_y around the final axis $y//y2$ (final frame $R(x, y, z)$).

Which rotation vector of the frame R relative to R_s expressed in R

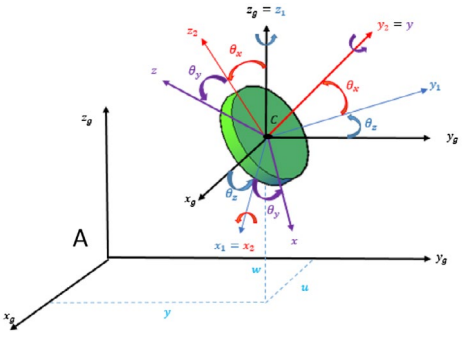

Figure 2. Intermediate frame used to move from frame R_s linked to the support frame R related to the deformed shaft.

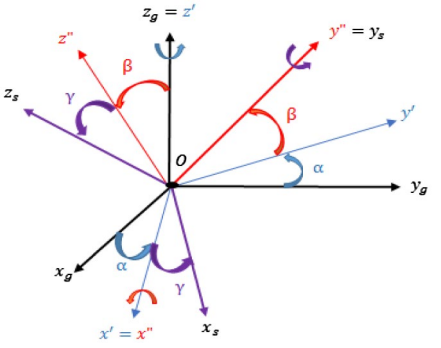

Figure 3. Intermediate frame, transition from Galilean reference R_g to frame R_s linked to the support.

$$\vec{\Omega}_R^{Rs} = \begin{bmatrix} 0 \\ 0 \\ \dot{\theta}_z \end{bmatrix}_{R_s} + \begin{bmatrix} \dot{\theta}_x \\ 0 \\ 0 \end{bmatrix}_{R_2} + \begin{bmatrix} 0 \\ \dot{\theta}_y \\ 0 \end{bmatrix}_{R} \tag{1.2}$$

$$\vec{\Omega}_R^{Rs} = \begin{bmatrix} \dot{\theta}_x \cos\theta_y - \dot{\theta}_z \cos\theta_x \sin\theta_y \\ \dot{\theta}_y + \dot{\theta}_z \sin\theta_x \\ \dot{\theta}_x \sin\theta_y + \dot{\theta}_z \cos\theta_x \cos\theta_y \end{bmatrix}_R \tag{1.3}$$

The motion of the base is defined by the coordinates x_A, y_A, and z_A, of the vector $\overrightarrow{OA}$ expressed in the frame R_g, and by the angles α, β, and γ which allow to go from frame R_g to frame R_s (see Figure 3):

- a rotation angle α around z_g (intermediate frame $R'(x', y', z')$)
- a rotation angle β around the new axis x' (intermediate frame $R''(x'', y'', z'')$)
- a rotation angle γ around the final axis $y'' = y_s$ (final frame $R_s(x_s, y_s, z_s)$)

Knowing that the rotations α, β, and γ depend on time t (Figure 4).

The rotation vector of the frame R_s compared to R_g expressed in R_s is written as,

$$\vec{\Omega}_{R_s}^{R_g} = \begin{bmatrix} 0 \\ 0 \\ \dot{\alpha} \end{bmatrix}_{R'} + \begin{bmatrix} \dot{\beta} \\ 0 \\ 0 \end{bmatrix}_{R''} + \begin{bmatrix} 0 \\ \dot{\gamma} \\ 0 \end{bmatrix}_{R_s} \tag{1.4}$$

$$\vec{\Omega}_{R_s}^{R_g} = \begin{bmatrix} \dot{\beta}\cos\gamma - \dot{\alpha}\cos\beta\sin\gamma \\ \dot{\gamma} + \dot{\alpha}\sin\beta \\ \dot{\beta}\sin\gamma + \dot{\alpha}\cos\beta\cos\gamma \end{bmatrix}_{R_s} = \begin{bmatrix} \dot{\alpha}_s \\ \dot{\beta}_s \\ \dot{\gamma}_s \end{bmatrix}_{R_s} \tag{1.5}$$

To configure the translation movements of the support, the coordinates X, Y, Z of the vector $\overrightarrow{OA}$ expressed in frame R_s are used (Duchemin et al., 2006).

$$\overrightarrow{OA} = \begin{bmatrix} \left(x_A\cos\alpha + y_A\sin\alpha\right)\cos\gamma - \left(z_A\cos\beta + \left(x_A\sin\alpha - y_A\cos\alpha\right)\sin\beta\right)\sin\gamma \\ z_A\sin\beta - \left(x_A\sin\alpha - y_A\cos\alpha\right)\cos\beta \\ \left(x_A\cos\alpha + y_A\sin\alpha\right)\sin\gamma + \left(z_A\cos\beta + \left(x_A\sin\alpha - y_A\cos\alpha\right)\sin\beta\right)\cos\gamma \end{bmatrix}_{R_s} = \begin{bmatrix} X \\ Y \\ Z \end{bmatrix} \tag{1.6}$$

Starting from the equations of motion of the support expressed in the Galilean reference R_g, the rotation vector coordinates and position of the frame R with respect to R_g can be obtained easily. For the following developments, equations are expressed in terms of $\dot{\alpha}_s$, $\dot{\beta}_s$, $\dot{\gamma}_s$ and X, Y, Z and their derivatives with respect to time.

The rotation vector of frame R with respect to frame R_g is :

$$\vec{\Omega}_R^{R_g} = \vec{\Omega}_{R_s}^{R_g} + \vec{\Omega}_R^{Rs} = \begin{bmatrix} \dot{\alpha}_s \\ \dot{\beta}_s \\ \dot{\gamma}_s \end{bmatrix}_{R_s} + \begin{bmatrix} 0 \\ 0 \\ \dot{\theta}_z \end{bmatrix}_{R_s} + \begin{bmatrix} \dot{\theta}_x \\ 0 \\ 0 \end{bmatrix}_{R_2} + \begin{bmatrix} 0 \\ \dot{\theta}_y \\ 0 \end{bmatrix}_{R} \tag{1.7}$$

$$\vec{\Omega}_R^{R_g} = \begin{bmatrix} \left(\dot{\alpha}_s\cos\theta_z + \dot{\beta}_s\sin\theta_z + \dot{\theta}_x\right)\cos\theta_y - \left(\left(\dot{\alpha}_s\sin\theta_z - \dot{\beta}_s\cos\theta_z\right)\sin\theta_x + \left(\dot{\gamma}_s + \dot{\theta}_y\right)\cos\theta_x\right)\sin\theta_y \\ -\left(\dot{\alpha}_s\sin\theta_z - \dot{\beta}_s\cos\theta_z\right)\cos\theta_x + \left(\dot{\gamma}_s + \dot{\theta}_y\right)\sin\theta_x + \dot{\theta}_y \\ \left(\dot{\alpha}_s\cos\theta_z + \dot{\beta}_s\sin\theta_z + \dot{\theta}_x\right)\sin\theta_y + \left(\left(\dot{\alpha}_s\sin\theta_z - \dot{\beta}_s\cos\theta_z\right)\sin\theta_x + \left(\dot{\gamma}_s + \dot{\theta}_y\right)\cos\theta_x\right)\cos\theta_y \end{bmatrix}_R \tag{1.8}$$

$$\vec{\Omega}_R^{R_g} = \begin{bmatrix} \omega_x \\ \omega_y \\ \omega_z \end{bmatrix} \tag{1.9}$$

The rotor rotation speed is along the axis y; θ_z and θ_x represent the angular deformation of the shaft in directions x and z; θ_y represents its angular position relative to the support. The shaft undergoes only small deformations (elastic domain), θ_z and θ_x are considered infinitely small angles.

Based on the assumptions, the rotor rotates at constant speed $\dot{\theta}_y$:

$$\dot{\theta}_y = \Omega \text{ and } \theta_y = \Omega\, t \tag{1.10}$$

Let (u, y, w) be displacement of a point C of the shaft in frame R_s, u and w are variables where y is considered constant since only the shaft deflection movements are studied, so:

$$\overrightarrow{\mathrm{AC}} = \begin{bmatrix} u(y,t) \\ y \\ w(y,t) \end{bmatrix}_{R_s} \tag{1.11}$$

And the velocity vector of point C relative to the Galilean reference is:

$$\vec{V}^g(C) = \frac{\mathrm{d}^g}{\mathrm{d}t}\overrightarrow{\mathrm{OC}} = \frac{\mathrm{d}^s}{\mathrm{d}t}\overrightarrow{\mathrm{OC}} + \vec{\Omega}_{R_s}^{R_g} \wedge \overrightarrow{\mathrm{OC}} \text{ avec } \overrightarrow{\mathrm{OC}} = \overrightarrow{\mathrm{OA}} + \overrightarrow{\mathrm{AC}} = \begin{bmatrix} X + u(y,t) \\ Y + y \\ Z + w(y,t) \end{bmatrix} \tag{1.12}$$

$$\vec{V}^g(C) = \begin{bmatrix} \dot{X} + \dot{u} \\ \dot{Y} \\ \dot{Z} + \dot{w} \end{bmatrix}_{R_s} + \begin{bmatrix} \dot{\alpha}_s \\ \dot{\beta}_s \\ \dot{\gamma}_s \end{bmatrix}_{R_s} \wedge \begin{bmatrix} X + u \\ Y + y \\ Z + w \end{bmatrix}_{R_s} \tag{1.13}$$

$$\vec{V}^g(C) = \begin{bmatrix} \dot{X} + \dot{u} + \dot{\beta}_s(Z + w) - \dot{\gamma}_s\left(Y + y\right) \\ \dot{Y} + \dot{\gamma}_s(X + u) - \dot{\alpha}_s(Z + w) \\ \dot{Z} + \dot{w} + \dot{\alpha}_s\left(Y + y\right) - \dot{\beta}_s(X + u) \end{bmatrix} = \begin{bmatrix} u_c \\ v_c \\ w_c \end{bmatrix} \tag{1.14}$$

The terms of the kinetic energies of the shaft and the disc can be calculated from the expressions of the rotation vector $\vec{\Omega}_R^{R_g}$ and the velocity of point C with respect to frame R_g

2.1.1. Disc kinetic energy

In general case, the disc is assumed to be perfectly rigid and only its kinetic energy is taken, the disc centre C is located at the arbitrary position y_d (Figure 1). Its kinetic energy is written as:

$$E_D = \frac{1}{2} m_d \left(\vec{V}^g(C)\right)^2 + \frac{1}{2}\vec{\Omega}_R^{R_g} I_c \vec{\Omega}_R^{R_g} \tag{1.15}$$

where m_d is the mass of the disc and I_c is its principal inertia tensor expressed in the frame related to the disc:

$$I_c = \begin{bmatrix} I_{dx} & 0 & 0 \\ 0 & I_{dy} & 0 \\ 0 & 0 & I_{dz} \end{bmatrix} \tag{1.16}$$

If the disc is symmetrical: $I_{dx} = I_{dz}$, then the kinetic energy is:

$$E_D = \frac{1}{2} m_d \left(u_c^2 + v_c^2 + w_c^2\right) + \frac{1}{2}\left(I_{dx}\omega_x^2 + I_{dy}\omega_y^2 + I_{dz}\omega_z^2\right) \tag{1.17}$$

To distinguish the effects due to the inertia of the average section of the disc and the effects of the asymmetry, the following notation is used:

$$I_{m_d}^{m_o} = \frac{I_{dx} + I_{dz}}{2}, \quad I_{m_d}^{di} = \frac{I_{dx} - I_{dz}}{2}, \quad I_{m_d}^{y} = I_{dy} \tag{1.18}$$

The kinetic energy of the disc is then written as:

$$E_d = \frac{1}{2} m_d t_1(y,t) + \frac{1}{2}\left[I_{m_d}^{m_o} t_2(y,t) + I_{m_d}^{y} t_3(y,t) + I_{m_d}^{di} t_4(y,t)\right] \tag{1.19}$$

With:

$$\begin{aligned} t_1(y,t) &= u_c^2 + v_c^2 + w_c^2 \\ t_2(y,t) &= \omega_x^2 + \omega_z^2 \\ t_3(y,t) &= \omega_y^2 \\ t_4(y,t) &= \omega_x^2 - \omega_z^2 \end{aligned} \tag{1.20}$$

The final expression of the kinetic energy E_d of the mass centre of disc placed at the arbitrary abscissa y_d along the axis O_y of the frame related to the support R is :

$$E_d = E_{d,1} + E_{d,2} + E_{d,3} + E_{d,4} \tag{1.21}$$

$$\begin{aligned} E_{d,1} \;=\; & \tfrac{1}{2} m_d \Big(\left(\dot{x}_0 + z_0\omega^y - \left(y_0 + y_d\right)\omega^z\right)^2 + \left(\dot{y}_0 - z_0\omega^x + x_0\omega^z\right)^2 \\ & + \left(\dot{z}_0 + \left(y_0 + y_d\right)\omega^x - x_0\omega^y\right)^2 + \dot{u}_d^2 + \dot{w}_d^2 \\ & + 2\left(\left(\dot{x}_0 + z_0\omega^y - \left(y_0 + y_d\right)\omega^z\right)\right)\left(\dot{u}_d + w_d\omega^y\right) \\ & + 2\left(\left(\dot{z}_0 + \left(y_0 + y_d\right)\omega^x - x_0\omega^y\right)\right)\left(\dot{w}_d - u_d\omega^y\right) \\ & - 2\left(\left(\dot{y}_0 - z_0\omega^x + x_0\omega^z\right)\right)\left(w_d\omega^x - u_d\omega^z\right) + 2\left(\dot{u}_d w_d - \dot{w}_d u_d\right)\omega^y \\ & + w_d^2\omega^{x^2} + \left(u_d^2 + w_d^2\right)\omega^{y^2} + u_d^2\omega^{z^2} - 2u_d w_d\omega^x\omega^z \Big) \end{aligned} \tag{1.22}$$

$$\begin{aligned} E_{d,2} &= \tfrac{1}{2} I_{m_d}^{m_o}\Big(\dot\theta_z^2 + \dot\theta_x^2 + 2\dot\theta_x\omega^x - 2\big(\dot\theta_z\theta_x - \dot\theta_x\theta_z\big)\omega^y + 2\dot\theta_z\omega^z - \big(\theta_z^2 - 1\big)\omega^{x^2} \\ &\quad + \big(\theta_z^2 + \theta_x^2\big)\omega^{y^2} - \big(\theta_x^2 - 1\big)\omega^{z^2} + 2\theta_z\theta_x\omega^x\omega^z + 2\big(\theta_z\omega^x - \theta_x\omega^z\big)\omega^y\Big) \end{aligned} \tag{1.23}$$

$$\begin{aligned} E_{d,3} = \frac{1}{2} I_{m_d}^{y}\Big(&(\Omega + \omega^y)^2 + \theta_z^2\omega^{x^2} + \theta_x^2\omega^{z^2} + (\Omega + \omega^y) \\ &\times \big(2\dot\theta_z\theta_x - \big(\theta_z^2 + \theta_x^2\big)\omega^y - 2\big(\theta_z\omega^x - \theta_x\omega^z\big)\big) - 2\theta_z\theta_x\omega^x\omega^z\Big) \end{aligned} \tag{1.24}$$

$$\begin{aligned} E_{d,4} &= -\tfrac{1}{2} I_{m_d}^{di}\Big(\dot\theta_z^2 - \dot\theta_x^2 - 2\dot\theta_x\omega^x - 2\big(\dot\theta_z\theta_x + \dot\theta_x\theta_z\big)\omega^y + 2\dot\theta_z\omega^z + \big(\theta_z^2 - 1\big)\omega^{x^2} \\ &\quad - \big(\theta_z^2 - \theta_x^2\big)\omega^{y^2} - \big(\theta_x^2 - 1\big)\omega^{z^2} + 2\theta_z\theta_x\omega^x\omega^z \\ &\quad - 2\big(\theta_z\omega^x + \theta_x\omega^z\big)\omega^y\big)\cos 2\Omega t \\ &\quad - \tfrac{1}{2} I_{m_d}^{di}(2\dot\theta_z\dot\theta_x + 2\dot\theta_z\omega^x + 2\big(\dot\theta_z\theta_z - \dot\theta_x\theta_x\big)\omega^y + 2\dot\theta_x\omega^z \\ &\quad + 2\theta_z\theta_x\Big(\omega^{x^2} - \omega^{y^2}\Big) - \big(\theta_z^2 + \theta_x^2 - 2\big)\omega^x\omega^z \\ &\quad - 2\big(\theta_x\omega^x - \theta_z\omega^z\big)\omega^y\Big)\sin 2\Omega t \end{aligned} \tag{1.25}$$

2.1.2. Shaft energies

The shaft is supposed to be deformable. It is necessary to calculate both its kinetic energy and its strain energy.

- Kinetic energy

The kinetic energy of a shaft element dE_a can be derived by extension of the kinetic energy of the disc considering an infinitely thin shaft section, with a thickness dy, and section S_a (supposed to be constant), density ρ_a and Section inertia I_{ax} and I_{az} (also assumed to be constant).

Elementary kinetic energy of an infinitely thin shaft section is then:

$$dE_a = \left(\frac{\rho_a S_a}{2}\big(u_c^2 + v_c^2 + w_c^2\big) + \frac{1}{2}\Big(\rho_a I_{\text{ax}}\omega_x^2 + \rho_a\big(I_{\text{ax}} + I_{\text{az}}\big)\omega_y^2 + \rho_a I_{\text{az}}\omega_z^2\Big)\right)dy \tag{1.26}$$

When the shaft is not symmetrical ($I_{\text{ax}} \neq I_{\text{az}}$), it has the following amounts:

$$I_{s_a}^{m_o} = \frac{I_{ax} + I_{az}}{2}, \quad I_{s_a}^{di} = \frac{I_{ax} - I_{az}}{2} \tag{1.27}$$

$$\begin{aligned} E_a &= \tfrac{\rho_a S_a}{2}\int_0^{l_a} t_1\big(y,t\big)dy \\ &\quad + \tfrac{1}{2}\Big(\rho_a I_{s_a}^{m_o}\int_0^{l_a} t_2\big(y,t\big)dy + 2\rho_a I_{s_a}^{m_o}\int_0^{l_a} t_3\big(y,t\big)dy + \rho_a I_{s_a}^{di}\int_0^{l_a} t_4\big(y,t\big)dy\Big) \end{aligned} \tag{1.28}$$

The development of Equation (1.28) leads to the final expression for the kinetic energy:

$$E_a = E_{a,1} + E_{a,2} + E_{a,3} + E_{a,4} \tag{1.29}$$

$$\begin{aligned} E_{a,1} \;=\; & \tfrac{\rho_a S_a}{2} \int_0^{l_a} \Big(\big(\dot{x}_0 + z_0\omega^y - \big(y_0 + y\big)\omega^z\big)^2 + \big(\dot{y}_0 - z_0\omega^x + x_0\omega^z\big)^2 \\ & + \big(\dot{z}_0 + \big(y_0 + y\big)\omega^x - x_0\omega^y\big)^2 + \dot{u}^2 + \dot{w}^2 \\ & + 2\big(\big(\dot{x}_0 + z_0\omega^y - \big(y_0 + y\big)\omega^z\big)\big)(\dot{u} + w\omega^y) \\ & + 2\big(\big(\dot{z}_0 + \big(y_0 + y\big)\omega^x - x_0\omega^y\big)\big)(\dot{w} - u\omega^y) \\ & - 2\big(\big(\dot{y}_0 - z_0\omega^x + x_0\omega^z\big)\big)\big(w\omega^x - u\omega^z\big) + 2(\dot{u}w - \dot{w}u)\omega^y + w^2\omega^{x^2} \\ & + \big(u^2 + w^2\big)\omega^{y^2} + u^2\omega^{z^2} - 2uw\omega^x\omega^z \Big) \mathrm{d}y \end{aligned} \tag{1.30}$$

$$\begin{aligned} E_{a,2} \;=\; & \tfrac{\rho_a I_{s_a}^{m_o}}{2} \int_0^{l_a} \Big(\dot{\theta}_z^2 + \dot{\theta}_x^2 + 2\dot{\theta}_x\omega^x - 2\big(\dot{\theta}_z\theta_x - \dot{\theta}_x\theta_z\big)\omega^y + 2\dot{\theta}_z\omega^z - \big(\theta_z^2 - 1\big)\omega^{x^2} \\ & + \big(\theta_z^2 + \theta_x^2\big)\omega^{y^2} - \big(\theta_x^2 - 1\big)\omega^{z^2} + 2\theta_z\theta_x\omega^x\omega^z \\ & + 2\big(\theta_z\omega^x - \theta_x\omega^z\big)\omega^y\big) dy \end{aligned} \tag{1.31}$$

$$\begin{aligned} E_{a,3} \;=\; & \rho_a I_{s_a}^{m_o} \int_0^{l_a} \Big((\Omega + \omega^y)^2 + \theta_z^2\omega^{x^2} + \theta_x^2\omega^{z^2} \\ & + (\Omega + \omega^y)\big(2\dot{\theta}_z\theta_x - \big(\theta_z^2 + \theta_x^2\big)\omega^y - 2\big(\theta_z\omega^x - \theta_x\omega^z\big)\big) \\ & - 2\theta_z\theta_x\omega^x\omega^z\Big) dy \end{aligned} \tag{1.32}$$

$$\begin{aligned} E_{a,4} \;=\; & -\tfrac{1}{2}\rho_a I_{s_a}^{di} \int_0^{l_a} \Big(\dot{\theta}_z^2\dot{\theta}_x^2 - 2\dot{\theta}_x\omega^x - 2\big(\dot{\theta}_z\theta_x + \dot{\theta}_x\theta_z\big)\omega^y + 2\dot{\theta}_z\omega^z + \big(\theta_z^2 - 1\big)\omega^{x^2} \\ & - \big(\theta_z^2 - \theta_x^2\big)\omega^{y^2} - \big(\theta_x^2 - 1\big)\omega^{z^2} + 2\theta_z\theta_x\omega^x\omega^z \\ & - 2\big(\theta_z\omega^x + \theta_x\omega^z\big)\omega^y\big) dy \;\cos 2\Omega t \\ & - \tfrac{1}{2}\rho_a \int_0^{l_a} I_{s_a}^{di} (2\dot{\theta}_z\dot{\theta}_x + 2\dot{\theta}_z\omega^x + 2\big(\dot{\theta}_z\theta_z - \dot{\theta}_x\theta_x\big)\omega^y \\ & + 2\dot{\theta}_x\omega^z + 2\theta_z\theta_x\Big(\omega^{x^2} - \omega^{y^2}\Big) - \big(\theta_z^2 + \theta_x^2 - 2\big)\omega^x\omega^z \\ & - 2\big(\theta_x\omega^x - \theta_z\omega^z\big)\omega^y\big) dy \;\sin 2\Omega t \end{aligned} \tag{1.33}$$

- Strain energy

The strain energy is not affected by the movement of the support because it only depends on the constraints and therefore the deformation of the shaft with respect to the support. In this calculation, only the deformations due to bending is taken into account (the effects of shear are neglected) (Dakel, 2013).

In the case of an Euler–Bernoulli beam, shear effects are neglected and relationships between rotations θ_z and θ_x supposedly small and u and w displacements are expressed by:

$$\theta_z = -\frac{\partial u}{\partial y}, \quad \theta_x = \frac{\partial w}{\partial y} \tag{1.34}$$

$$\begin{aligned} U_a &= \tfrac{1}{2}E_a I_{S_a}^{m_o} \int_0^{l_a} \left(\left(\frac{\partial^2 u}{\partial y^2}\right)^2 + \left(\frac{\partial^2 w}{\partial y^2}\right)^2 \right) dy \\ &\quad - \tfrac{1}{2}E_a I_{S_a}^{di} \int_0^{l_a} \left(\left(\frac{\partial^2 u}{\partial y^2}\right)^2 - \left(\frac{\partial^2 w}{\partial y^2}\right)^2 \right) dy \cos 2\Omega t \\ &\quad + E_a I_{S_a}^{di} \int_0^{l_a} \frac{\partial^2 u}{\partial y^2}\frac{\partial^2 w}{\partial y^2} dy \sin 2\Omega \\ &\quad + \tfrac{1}{4}\rho_a S_a \int_0^{l_a} ((la) - y^2) \left(\left(\frac{\partial u}{\partial y}\right)^2 + \left(\frac{\partial w}{\partial y}\right)^2 \right) dy \left(\omega^{x2} + \omega^{z2}\right) \end{aligned} \tag{1.35}$$

3. Modelling of the rotor with the h-p version of the finite element

In the h-p version of the finite element method, with an assembly of the same way as the conventional version of the finite element method for multiple items, the error can be controlled not only by refining the mesh, but also by increasing the degree of shape functions (polynomial of degree p) of all elements (Lin & Hsiao, 2001).

In our study, we use the method of hierarchical finite elements with polynomial shape functions K-orthogonal generated by the Legendre differential equation (Bardell, 1996), combined with the classic method of finite elements, ensuring compatibility between the two versions. The rotating shaft is modelled by hierarchical 3D beam elements with Euler–Bernoulli beam type Each element is shown in Figures 4 and 5 with two nodes 1 and 2. In case of a stepped shaft, several elements may be used.

Local coordinates are related to the non-dimensional coordinates by the equation:

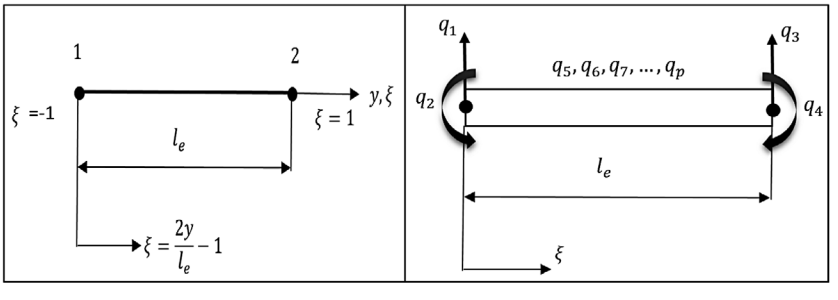

Figure 4. Bar element with two nodes (nodes and internal displacement).

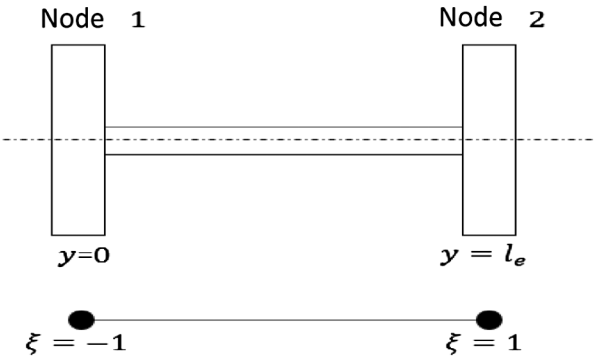

Figure 5. Positions of the disc into the shaft (one element).

$$\xi = \frac{2y}{l_a} - 1 \quad \text{with} \ -1 \leq \xi \leq 1 \tag{2.1}$$

In p version of the finite elements, the group of shape functions is composed of two parts,

$$\left[f_1, f_2, f_3, f_4, \ldots, f_p\right] \tag{2.2}$$

The first four functions are those of the finite element necessary for the description of displacement q_1, q_3, and rotations q_2, q_4 at the nodes of the element, so we use cubic Hermit shape functions (Bardell, 1996).

$$\begin{cases} f_1(\xi) = \frac{1}{2} - \frac{3}{4}\xi + \frac{1}{4}\xi^3 \\ f_2(\xi) = \left(\frac{1}{8} - \frac{1}{8}\xi - \frac{1}{8}\xi^2 + \frac{1}{8}\xi^3\right) l_e \\ f_3(\xi) = \frac{1}{2} + \frac{3}{4}\xi - \frac{1}{4}\xi^3 \\ f_4(\xi) = \left(-\frac{1}{8} - \frac{1}{8}\xi + \frac{1}{8}\xi^2 + \frac{1}{8}\xi^3\right) l_e \end{cases} \tag{2.3}$$

The other shape functions up to the maximum number of polynomial degree taken p, are the functions contributing to the internal displacement field, and are polynomial K-orthogonal type.

For this particular problem, there is a great advantage in the search for a set of hierarchical shape functions that are orthogonal second derivative, both for themselves and the four original cubic Hermit functions. Such an assembly may be derived from the form of special Rodrigues Legendre polynomials (Peano, 1976); the generating function is mentioned below.

$$f_r(\xi) = \sum_{n=0}^{\frac{(r-1)}{2}} \frac{(-1)^n (2r - 2n - 7)!!}{2^n n! (r - 2n - 1)!} \xi^{(r-2n-1)} \tag{2.4}$$

$$\begin{gathered}\text{with } r > 4 \\ r!! = r(r-2)(r-4)\ldots(2 \text{ or } 1), \quad 0!! = (-1)!! = 1, \\ (r-1)/2 \text{ Designates its own whole part}\end{gathered} \tag{2.5}$$

The vector of generalised displacements is given by:

$$\{q\} = \{q_u, q_w\}^T \tag{2.6}$$

$$\begin{cases} \{q_u\} = \left\{x_1, x_2, x_3, \ldots, x_{p_u}\right\}^T \exp\left(j\omega t\right) \\ \{q_w\} = \left\{z_1, z_2, z_3, \ldots, z_{p_w}\right\}^T \exp\left(j\omega t\right) \end{cases} \tag{2.7}$$

The vector of generalised displacements is given by:

$$\begin{cases} u = \left[N_u\right]\{q_u\} = \sum_{m=1}^{p_u} x_m f_m(\xi) \exp\left(j\omega t\right) \\ w = \left[N_w\right]\{q_w\} = \sum_{m=1}^{p_w} z_m f_m(\xi) \exp\left(j\omega t\right) \end{cases} \tag{2.8}$$

The displacement vector {B} is given by:

$$\{\mathrm{B}\} = [N]\{q\} = \begin{Bmatrix} u \\ w \end{Bmatrix} = \begin{bmatrix} [N_u] & [0] \\ [0] & [N_w] \end{bmatrix} \begin{Bmatrix} \{q_u\} \\ \{q_w\} \end{Bmatrix} \tag{2.9}$$

where $[N]$ is the shape functions matrix

$$N_{u,w} = \left[f_1, f_2, f_3, f_4, \ldots, f_{p_u, p_w}\right] \tag{2.10}$$

3.1. Elementary matrices

To obtain the elementary matrices of the shaft according to the h-p version of the finite elements, we must make a change in Cartesian coordinates to no-dimensional coordinates, the introduction of the matrices of the shape functions, and the Euler–Lagrange equations are applied to obtain the following system of equations (Boukhalfa & Hadjoui, 2010):

$$\begin{aligned} &\frac{\mathrm{d}}{\mathrm{d}t}\left(\frac{\partial E_a}{\partial\{\dot{q}_t\}}\right) - \frac{\partial E_a}{\partial\{q_i\}} + \frac{\partial U_a}{\partial\{q_i\}} \\ &\quad = \left[M_{\mathrm{ea}}(t)\right]\{\ddot{q}_l\} + \left[C_{\mathrm{ea}}(t)\right]\{\dot{q}_l\} + \left[K_{\mathrm{ea}}(t)\right]\{q_i\} - \left\{F_{\mathrm{ea}}(t)\right\} \end{aligned} \tag{2.11}$$

$\left[M_{\mathrm{ea}}(t)\right]$, $\left[C_{\mathrm{ea}}(t)\right]$, $\left[K_{\mathrm{ea}}(t)\right]$ and $\left\{F_{\mathrm{ea}}(t)\right\}$ are the elementary matrices of mass, gyroscopic effect, rigidity and the vector of the excitation forces due to a carrier, respectively.

In the same manner as the shaft to obtain the elementary matrices of the disc, mass and gyroscopic stiffness of the support, by applying the Lagrange's equations on Equations (1.21–1.25), knowing that the disc is considered as a concentrated mass at a node (Figure 6).

We obtain the following matrices $[M_{ed}(t)]$, $[C_{ed}(t)]$, $[K_{ed}(t)]$, and $\{F_{ed}(t)\}$ which are: elementary mass matrices, gyroscopic, stiffness generated by the movement of the support and the vector of the excitation force of the disc generated by the movement of the support.

3.2. Elementary movement equation

Applying Lagrange equations to the discretised system by h-p version of the finite element method, we obtain the following differential equations:

$$[M_{er}(t)]\{\ddot{q}_r\} + [C_{er}(t)]\{\dot{q}_r\} + [K_{er}(t)]\{q_r\} = \{F_{er}(t)\} \tag{2.12}$$

where:

- $[M_{er}(t)]$, $[C_{er}(t)]$, and $[K_{er}(t)]$ are, respectively, the elementary matrices, mass, damping and stiffness, with periodical parametric terms and varying in time due to the geometric asymmetry of the rotating rotor and rotations of the rigid support.
- $\{\ddot{q}_r\}$, $\{\dot{q}_r\}$, and $\{q_r\}$ are, respectively, the acceleration vector, velocity and global displacement adapted to the connectivity of finite elements.
- $\{F_{er}(t)\}$ is the global vector of linear external forces containing excitations due to the rotational and linear movements of the support.

Matrices $[M_{er}(t)]$, $[C_{er}(t)]$, and $[K_{er}(t)]$ are defined as follows:

$$[M_{er}(t)] = [M_{ea}(t)] + [M_{ed}(t)] \tag{2.13}$$

$$[C_{er}(t)] = [C_{ea}(t)] + [C_{ed}(t)] \tag{2.14}$$

$$[K_{er}(t)] = [K_{ea}(t)] + [K_{ed}(t)] \tag{2.15}$$

The vector $\{F_{er}(t)\}$ is expressed by:

$$\{F_{er}(t)\} = \{F_{ea}(t)\} + \{F_{ed}(t)\} \tag{2.16}$$

4. Simulation and results

4.1. Symmetrical on-board rotor with rigid bearing

A computer programme for determining the natural modes of on-board rotor has been developed and for validate this programme, we have the rotor shown in Figure 6.

Table 1 shows the characteristics of symmetric rotor used in the literary Lalanne and Ferraris (1998), Duchemin et al. (2006), Dakel (2013).

In the Table 2 we find the features used for modelling with the finite element h-p version.

The symmetrical shaft is modelled by three identical finite element Euler–Bernoulli beam type. The symmetrical disc is located at node 2. The bearings are assumed to be rigid, generate a rotor-bearing at both ends and are located at nodes 1 and 4. Thus, the corresponding displacements are cancelled (Figure 6).

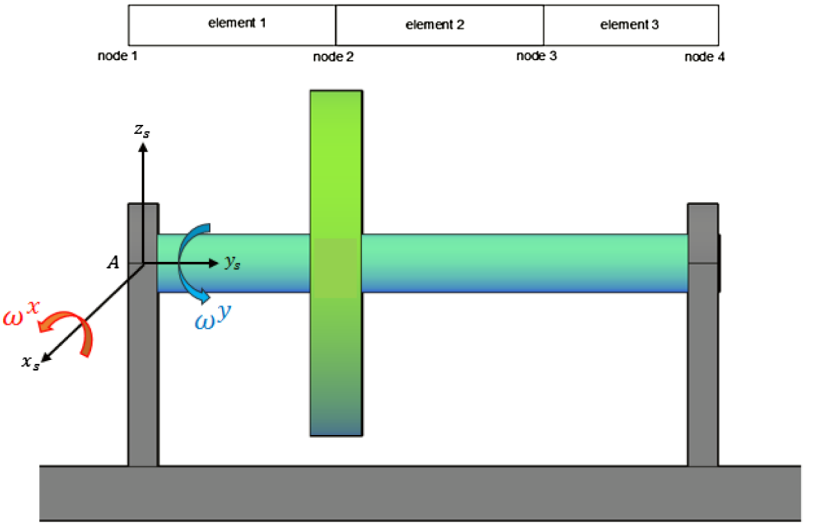

Figure 6. On-board symmetric rotor.

The rotor operates at a constant rotation speed Ω (rpm) and is subjected to the excitation of the constant rotary motion of the support: the rotation is constant around the axis O_x (or O_y) is given by ω^x (or ω^y). The equations of motion due to rotation ω^x of the support are shown in Equation (3.1) and those due to ω^y in Equation (3.2):

$$\begin{aligned}&\left([M]^a+[M]^d\right)\{\ddot{q}_r\}+\left(\left[C_g\right]^a+\left[C_g\right]^d\right)\Omega\{\dot{q}_r\}\\&+\left(\left[K_a^e\right]+\left(\left[K_a^{e.\omega^{x^2}}\right]+\left[K_\omega^{x^2}\right]^d+\left[K_\omega^{x^2}\right]^a\right)\omega^{x^2}\right)\{q_r\}\\&=\left\{F_{\mathrm{er}}(t)\right\}\end{aligned}\tag{3.1}$$

Table 1. Characteristics of symmetric rotor.

Density of the disc material	$\rho_d = 7800\ \text{kg/m}^3$
Outer radius of the disc	$r_d = .15\ \text{m}$
Disc thickness	$e_d = .03\ \text{m}$
Position of the disc	$y_d = .4/3\ \text{m}$
Density of the shaft material	$\rho_a = 7800\ \text{kg/m}^3$
Radius of the shaft	$r_a = .01\text{m}$
Length of the shaft	$l_a = .4\ \text{m}$
Young Module of the shaft	$E_a = 2 \times 10^{11}\ \text{N/m}^2$
Poisson coefficient of the shaft	$\upsilon_a = .3$

Table 2. Modelling features in version h-p finite element.

Number of elements	$n_{\text{el}} = 03$
Polynomial degree of elements	$p = 10$
Length of the elements	$l_e = l_a/n_{\text{el}}$

$$\left([M]^a + [M]^d\right)\{\ddot{q}_r\} + \left(\left(\left[C_g\right]^a + \left[C_g\right]^d\right)\Omega + \left(\left[C_{\omega^y}\right]^{a.\text{sup}} + \left[C_{\omega^y}\right]^{d.\text{sup}}\right)\omega^y\right)\{\dot{q}_r\}$$
$$+\left(\left[K_a^e\right] + \left(\left[K_{\Omega_{\omega^y}}\right]^a + \left[K_{\Omega_{\omega^y}}\right]^d\right)\Omega_{\omega^y} + \left(\left[K_{\omega^{y^2}}\right]^a + \left[K_{\omega^{y^2}}\right]^d\right)\omega^{y^2}\right)\{q_r\}$$
$$= \left\{F_{\text{er}}(t)\right\} \tag{3.2}$$

To demonstrate the basic phenomena occurring in rotor dynamics with the movements of the support and compare them to those related to the case of a fixed support, the analysis of the dynamic behaviour in continuous operation is performed through Campbell diagram.

Moreover, the equations of motion (3.1) and (3.2) of on-board rotor are assigned parametrically (left side of the equations) by rotations of the support, while the translations of the support only have an influence on the vector of the external forces (second member). The dynamic behaviour is completely analysed in accordance with the rotation of the support.

4.2. Campbell diagram

In the case where the rotor is symmetrical and subjected to a constant rotation of the support, the linear equations of motion (3.1) and (3.2) always have constant coefficients. It should be mentioned that a fixed support or a rotating support about the axis O_y leave the system isotropic, while rotation of the support about the axis O_x makes the system anisotropic. Furthermore, the sign of the components of damping and stiffness matrices depends on the direction and rotation of the support about O_y but not on the direction of the rotation of the support about O_x.

In the case of a positive direction (counter clockwise) of rotation of the support around O_y and any direction around de O_x, symmetrical stiffness matrices may lose their characteristic positive definite because of the presence of diagonal negative terms containing the angular velocity ω^x or ω^y.

To calculate the paper values of the system, we use Equations (3.1) and (3.2) without the second member, the results obtained are purely imaginary quantities

regardless of the constant angular velocity of rotation of the support in the area of interest ω^x or $\omega^y \in [0;10\ \text{Hz}]$, the on-board rotor is stable for all modal forms considered included within its operating speed range $\Omega \in [0;6000\ \text{tr min}]$.

Natural frequency f_r deduced from these eigenvalues depends on the speed of rotation Ω of the rotor and the angular velocity of rotation of the support about either O_x or O_y. They are represented with Campbell diagrams plotted in (Figure 10) for the rotor subjected to the angular velocity ω^x or ω^y. When the rotor of the support is fixed (ω^x or $\omega^y = 0$), the system is isotropic and therefore the dynamic behaviour of the rotor is symmetrical, that is to say, the natural frequencies of each pair of forward and reverse precession modes are equal at rest ($\boldsymbol{\Omega} = 0$). Even though the natural frequency does not change greatly, rotation ω^x(or ω^y) of the support generates an asymmetry in the behaviour of the rotor.

4.2.1. Interpretation of results and validation

A programme for calculating the natural frequencies and plotting Campbell diagrams was developed, using MATLAB programming language. After validating this programme, several examples were processed to determine the influence of angular perturbations of the support relative to the axes O_x and O_y and the locations of the discs on the rotor.

The results calculated in this article are handled with the h-p version of the finite elements method. It groups two methods, the classic version of the finite elements (h-FEM) and the p-version of the finite elements (p-FEM).

The advantage of using the h-p version of the finite element method in this paper is the ability to control both parameters of the previous versions (h-FEM and p-FEM). Knowing that if we fix the degree of polynomial in $p = 4$, and we vary the other one parametrizes (mesh degree h), the h-p version is converted into h version, and the found results are identical to those of the h version.

The same thing applies if we fix the mesh degree (h), and we vary the polynomial degree (p), the found results are similar to those of the p-version of the FEM.

In Figures 8–12, we proceeded as follows:

- Figures 8 and 11; we fix the number of elements (h-refinement) and we vary the polynomial degree-p.
- Figures 9 and 12; we fix the polynomial degree-p and we vary the number of elements (h-refinement).
- In the case of the Figure 10; we vary simultaneously both parameters (h-refinement and polynomial degree-p) using the following method: ($p_i = p_{i-1} + 1$ and $h_i = h_{i-1} * 2$).

4.2.2. Convergences of results

The results of the five bending modes for our model on-board rotor according to the number of shape functions are shown in Figure 7. The figure shows the rapid convergence to the exact values by increasing the number of shape functions. The

bending modes are identical for a number of hierarchical finite element equal to 3, it shows the accuracy of the method with a reduced number of the shape functions.

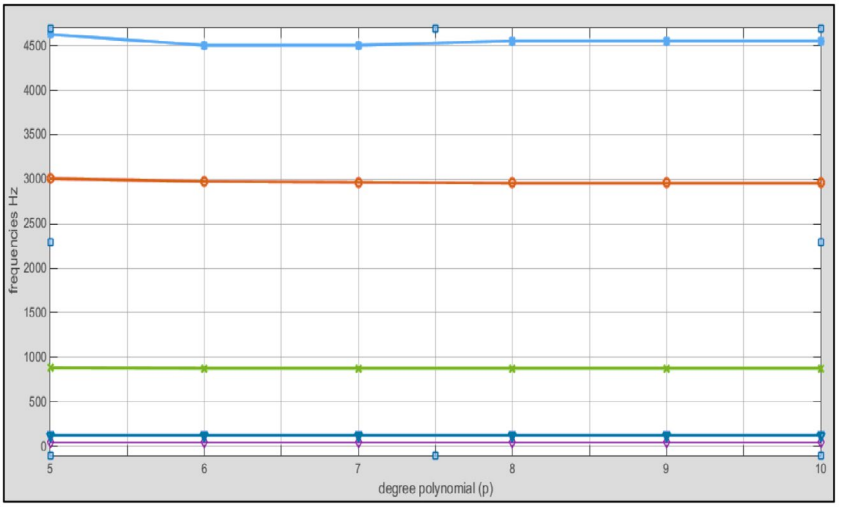

Figure 7. Convergence of the first five bending frequency according to the number of hierarchies of functions *p* (fixed support).

We notice that the convergence is very rapidly obtained for low frequencies (Figures 8 and 9) by increasing both parameters (*h* and *p*) of the version h-p. The gap between the results is very small and can be neglected; so to have good results for low frequencies, increasing the elements number (*h*-refinement) and the polynomial degree (*p*-refinement) are not necessary; we need to fix a parameter (either the number of elements -h or the polynomial degree-*p*) and varying the

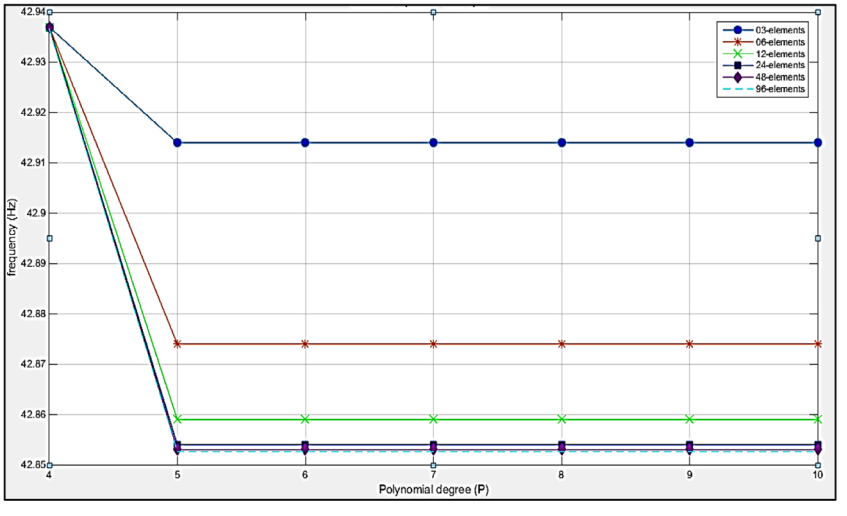

Figure 8. Convergence of the first frequency based on the number of *p* hierarchical shape functions with a fixed number of elements, at a speed of 1500 rpm.

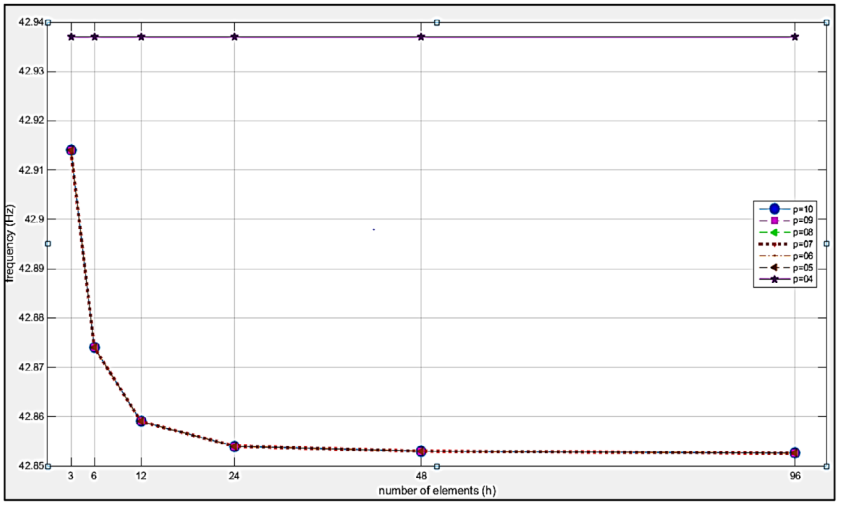

Figure 9. Convergence of the first frequency based on the number of elements (h), with a fixed polynomial degree (p) and a speed of 1500 rpm.

other one until the convergence is obtained. This phenomenon is generally valid for the low frequencies, between the first and the fifth one.

For high frequencies (Figures 11 and 12), starting from the sixth one, increasing the elements number (h-refinement) and the polynomial degree (p-refinement) are necessary and gives better results.

In the Figures 8 and 11, the curves of convergence are traced by the fixation of the mesh degree h and the variation of the polynomial degree p, we notice that more we increase the number of elements (h-refinement) more the gap between the curves of convergence decreases.

In case we fix the degree of polynomial p and we vary the mesh degree h (Figures 9 and 12), we notice that the convergence is very low(weak) in the case or $p = 4$ (which represents the h version of FEM), and in the case or $p \geq 5$ we have a fast convergence.

In Figure 10 we see that convergence is exponentially fast, However, we cannot provide a typical combination.

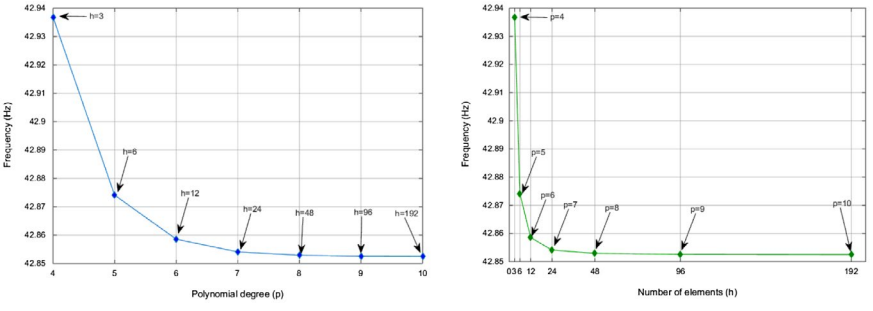

Figure 10. Convergence of the first frequency with a combination of the mesh degree-h and the polynomial degree-p with ($p_i = p_{i-1} + 1$ and $h_i = h_{i-1} \times 2$) in a 1500 rpm rotational speed.

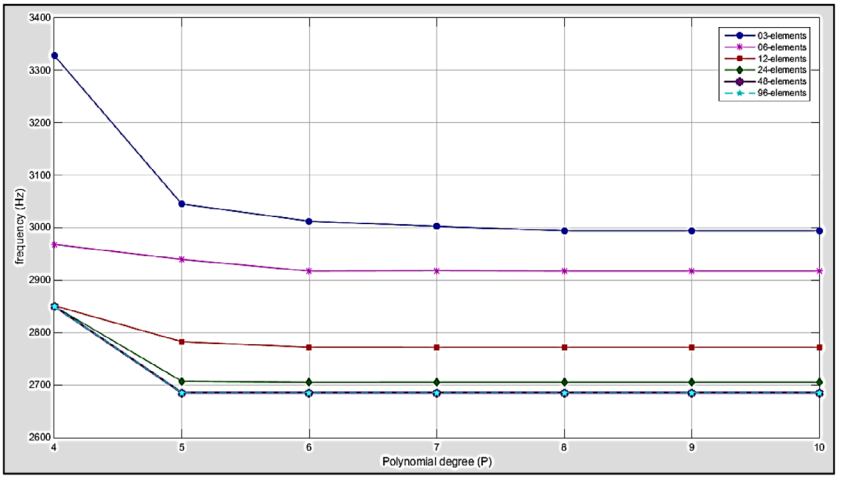

Figure 11. Convergence of the seventh frequency depending on the number of *p* hierarchical shape functions with a fixed number of elements, at a speed of 1500 rpm.

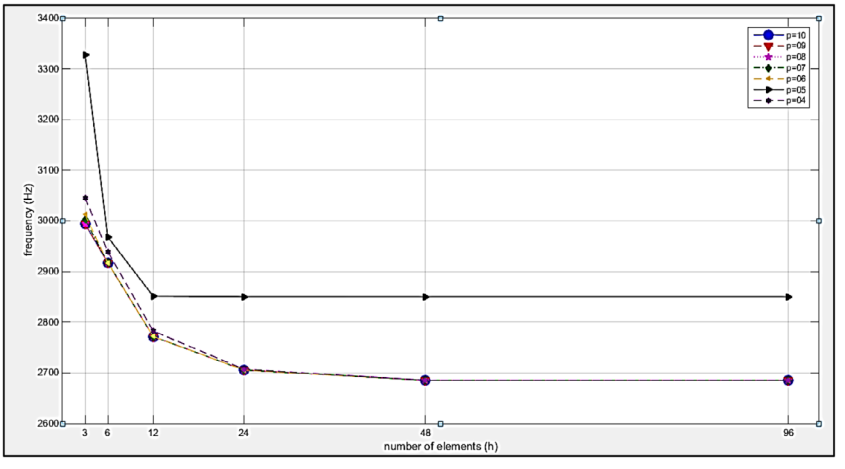

Figure 12. Convergence of the seventh frequency based on the number of elements (*h*), with a fixed polynomial degree (*p*) and a speed of 1500 rpm.

4.2.3. Interpretations of Campbell diagrams

Figure 13 shows the variation in the frequencies of the bending with versus the rotational speed (Campbell diagram) of the first two modes. The influence of the angular speed of the support taken in this example ($\omega^x = 0, 5, et\ 10$ Hz) is small, so better visualised the results on the graph, we used zooms in on two areas (see Figures 14 and 15).

We notice from these results that the influence of rotation of the support with respect to the O_x axis is very weak from the small angular rotations (5, 10 Hz), it is therefore concluded to have significant vibrations due to the rotation of the support along the O_x axis; these rotations must be as important.

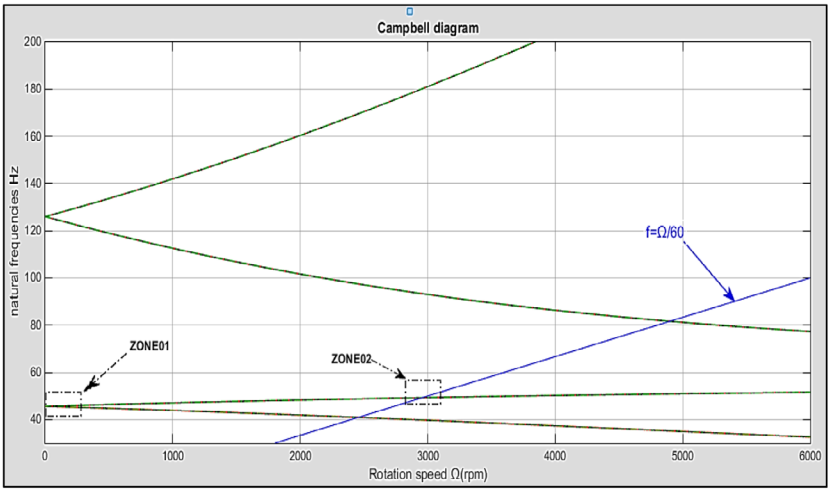

Figure 13. Campbell diagram for the first four frequencies of the rotor under the effect of the angular velocity of the support ($\omega^x = 0, 5, et\ 10\ Hz$).

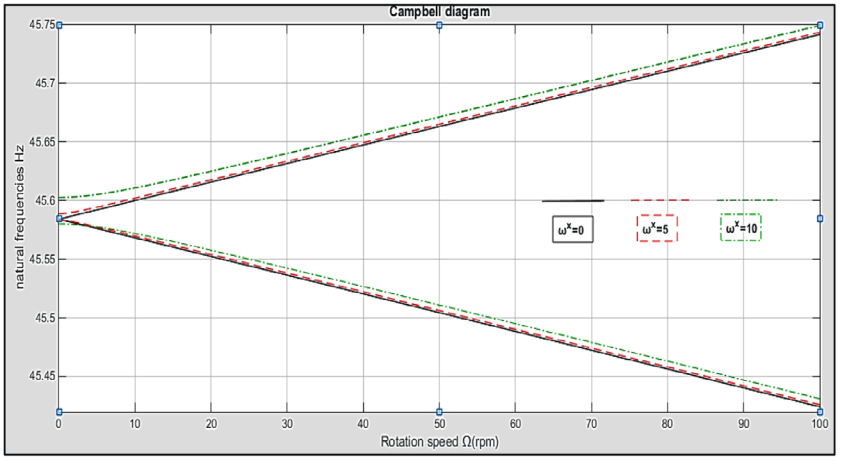

Figure 14. Expansion in zone 01 in Figure 12.

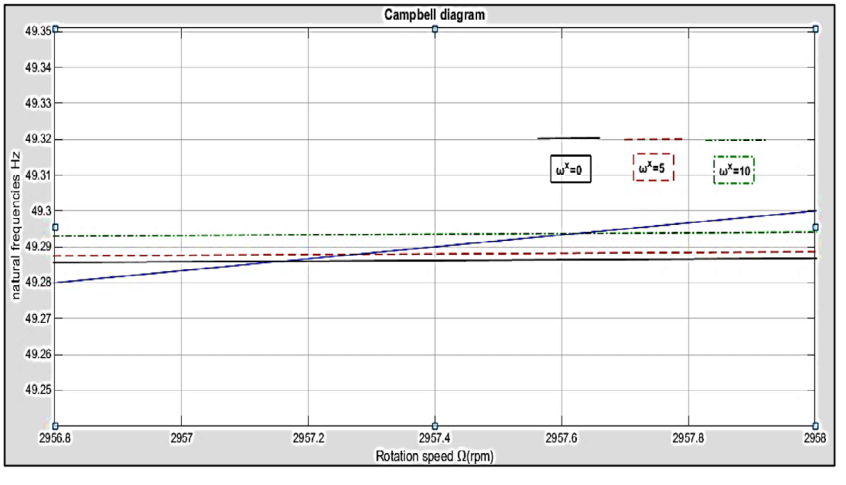

Figure 15. Expansion in zone 02 in Figure 12.

4.2.4. Comparison of results with other methods

- The case for a fixed support

In the Tables 3 and 4, we notice a slight gap of the results between both methods in spite of the difference of the taken finite elements number, for the classical finite element method, we took six elements, while in h-p version we took just three elements, all it took is just an increased degree of the polynomial (p). Convergence in the case of the finite element version h-p can be obtained by combining the number of elements h and the polynomial degree p. With a reduced number of elements, we have accurate results by increasing the degree of the polynomial.

- Table 5 represents the difference between the two methods when the support rotates at an angular velocity $\omega^x = 5, 10$ Hz about the axis O_x

We notice from Table 5, the h-p version of the finite element results is close to those of the classical version of the finite elements (h-FEM), knowing that in our example for version h-p it took only three elements and '10-degree' polynomial, while in the classical version we took six elements for the discretization of the shaft.

Table 3. Intersection of frequency curves with the line $f = \Omega/60$ in the Campbell diagram in the case where the support is fixed gives three critical speeds.

		FEM version-h	h-p version FEM
First indirect mode	Critical speed	2456.58 rpm	245.504 rpm
	Frequency	40.94 Hz	40.917 Hz
First direct mode	Critical speed	2959.17 rpm	2955.784 rpm
	Frequency	49.32 Hz	49.263 Hz
Second indirect mode	Critical speed	4899.23 rpm	4898.429 rpm
	Frequency	81.65 Hz	81.640 Hz

Table 4. Natural frequency depending on the rotational speed of the rotor and the fixed support (I and D is the reverse precision modes and direct respectively).

		Support fixed		
Ω (rpm)	f_r (Hz)	h-p version FEM	h-version FEM	h-p-FEM/h-FEM (ε%)
0	f_1^I	45.57	45.61	.09
	f_1^D	45.57	45.61	.09
	f_2^I	12.595	12.596	.00
	f_2^D	12.595	12.596	.00
1500	f_1^I	42.90	42.93	.06
	f_1^D	47.68	47.72	.09
	f_2^I	10.679	10.679	.00
	f_2^D	15.082	15.083	.01
3000	f_1^I	39.70	39.72	.05
	f_1^D	49.31	49.35	.09
	f_2^I	92.98	92.99	.01
	f_2^D	18.097	181	.02
4500	f_1^I	36.16	36.18	.04
	f_1^D	50.57	50.62	.11
	f_2^I	83.56	83.57	.01
	f_2^D	21.553	21.557	.02
6000	f_1^I	32.60	32.61	.04
	f_1^D	51.55	51.61	.11
	f_2^I	77.31	77.32	.02
	f_2^D	25.346	25.353	.03

Table 5. Natural frequency depending on the speed rotation of the rotor and the constant rotation of the support (*I* and *D* is the reverse precision and direct modes, respectively) $\omega^x = 0, 5, 10$ Hz.

		ω^x = 5 Hz			ω^x = 10 Hz		
Ω (rpm)	f_r (Hz)	h-p version	h-version	ε%	h-p version	h-version	ε%
0	f_1^I	45.583	45.610	.06	45.580	45.607	.06
	f_1^D	45.589	45.616	.06	45.603	45.629	.06
	f_2^I	125.992	125.960	.03	125.991	125.959	.03
	f_2^D	125.994	125.961	.03	125.999	125.967	.03
1500	f_1^I	42.915	42.938	.05	42.921	42.943	.05
	f_1^D	47.696	47.726	.06	47.702	47.731	.06
	f_2^I	106.811	106.793	.02	106.813	106.796	.02
	f_2^D	150.880	150.830	.03	150.882	150.832	.03
3000	f_1^I	39.711	39.729	.05	39.716	39.734	.05
	f_1^D	49.329	49.360	.06	49.334	49.365	.06
	f_2^I	92.996	92.990	.01	92.998	92.993	.01
	f_2^D	181.069	180.999	.04	181.071	181.002	.04
4500	f_1^I	36.170	36.183	.04	36.174	36.188	.04
	f_1^D	50.592	50.625	.06	50.598	50.629	.06
	f_2^I	83.570	83.575	.01	83.572	83.577	.01
	f_2^D	215.666	215.575	.04	215.668	215.577	.04
6000	f_1^I	32.599	32.609	.03	32.603	32.613	.03
	f_1^D	51.581	51.614	.06	51.587	51.619	.06
	f_2^I	77.311	77.324	.02	77.314	77.326	.02
	f_2^D	253.651	253.535	.05	253.653	253.537	.05

We also note that the behaviour of the rotor changes from the constant rotation of the rigid support which generates a slight asymmetry in the case of rotation around the O_x axis (ω^x), in this case it is concluded that the rotation of the support around the axis O_x (ω^x) does not affect a lot the behaviour of the rotor.

- Table 6 and the Figure 16 represent the difference between the two methods when the support rotates at an angular velocity ω^y around the axis O_y

Table 6. Natural frequency depending on the speed rotation of the rotor and the constant rotation of the support (*I* and *D* is the reverse precision and direct modes, respectively) $\omega^y = 5, 10$ Hz.

		ω^y = 5 Hz			ω^y = 10 Hz		
Ω (rpm)	f_r (Hz)	h-p version	h-version	ε%	h-p version	h-version	ε%
0	f_1^I	46.315	46.342	.06	47.068	47.095	.06
	f_1^D	44.875	44.903	.06	44.188	44.216	.06
	f_2^I	126.086	126.054	.03	125.801	126.146	.27
	f_2^D	125.898	125.864	.03	126.178	125.767	.33
1500	f_1^I	44.026	44.049	.05	45.149	47.761	5.47
	f_1^D	47.429	47.460	.06	47.183	50.028	5.69
	f_2^I	107.007	106.990	.02	107.209	107.470	.24
	f_2^D	150.825	150.775	.03	150.767	150.769	.00
3000	f_1^I	41.094	41.112	.04	42.460	46.860	9.39
	f_1^D	49.523	49.556	.07	49.725	55.169	9.87
	f_2^I	93.396	93.391	.00	93.816	94.890	1.13
	f_2^D	181.029	180.959	.04	180.985	180.961	.01
4500	f_1^I	37.696	37.709	.04	39.161	44.368	11.74
	f_1^D	51.248	51.282	.07	51.889	59.705	13.09
	f_2^I	84.293	84.299	.01	85.059	87.687	3.00
	f_2^D	215.630	215.538	.04	215.591	215.529	.03
6000	f_1^I	34.164	34.173	.03	35.617	40.859	12.83
	f_1^D	52.691	52.726	.07	53.758	63.747	15.67
	f_2^I	78.451	78.466	.02	79.655	84.414	5.64
	f_2^D	253.616	253.499	.05	253.577	253.478	.04

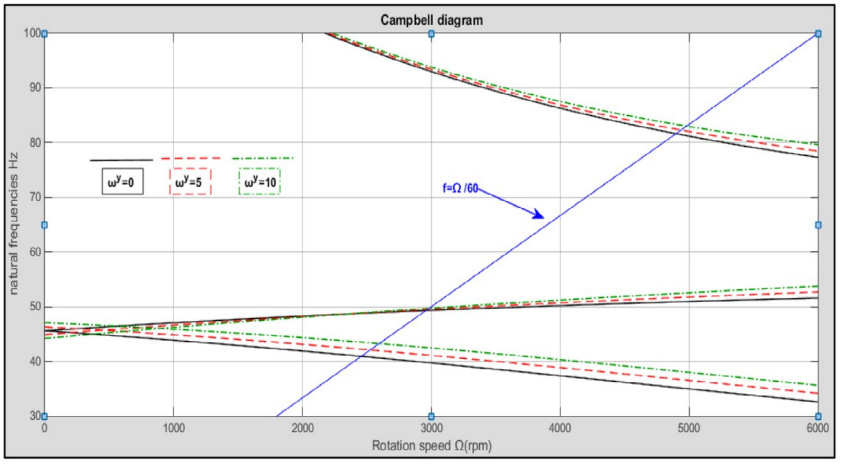

Figure 16. Campbell diagram for the first four frequencies of the rotor under the effect of the angular velocity of the support ($\omega^y = 0, 5, et$ 10 Hz).

We also notice that the behaviour of the rotor changes from the constant rotation of the rigid support which generates an asymmetry in the case of rotation around the axis O_y (ω^y), where we can see a large asymmetry, and amplification of the gyroscopic effect.

4.2.5. Influence of angular velocities of the mobile support on critical speeds

To confirm previous results, in Figures 17–19, we see the change in speed of the intersection of the first indirect mode (Figure 17) and direct (Figure 18) with the line $f = \Omega/60$ with respect to the rotation of the support around the axis O_x (ω^x) (ω^x = constant). We notice that the speed increases slightly even with big perturbations along the O_x axis.

However, for perturbations along the O_y axis, we see in Figure 18 the importance of the difference of critical velocities with respect to the rotation around the axis O_x ω^x(ω^x = constant).

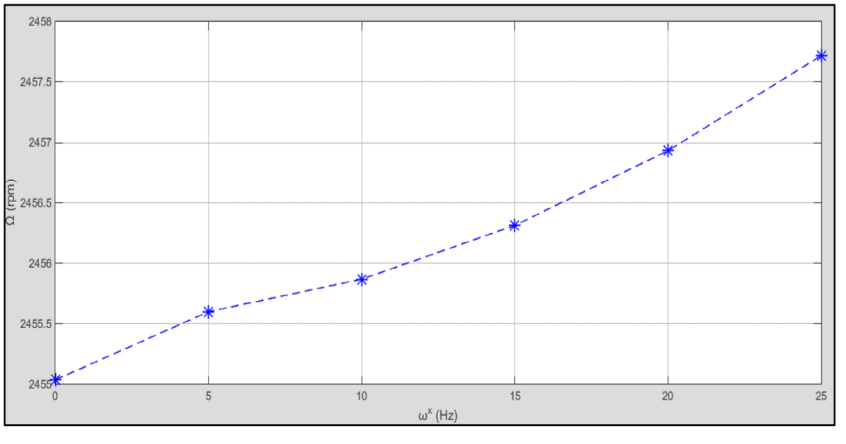

Figure 17. Speed of the intersection of the first indirect mode with the right $f = \Omega/60$ with respect to rotation of the support according to the axis O_x (ωx)(ωx = *constant).*

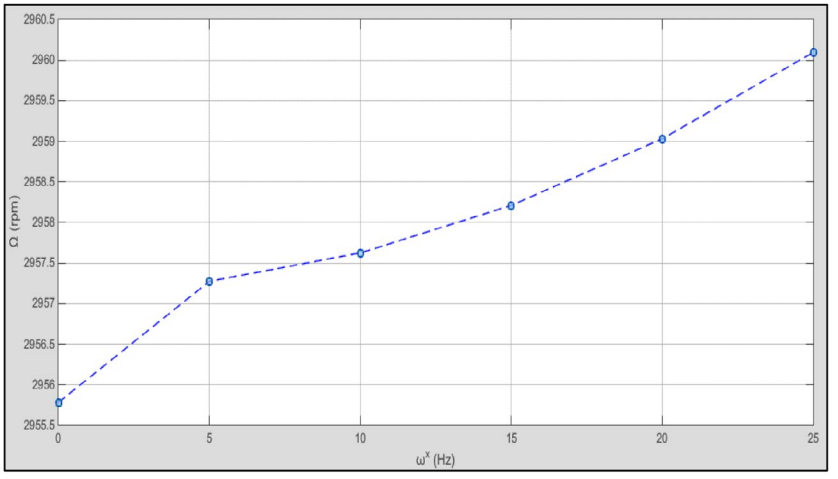

Figure 18. Speed of the intersection of the first direct mode with the right $f = \Omega/60$ with respect to rotation of the support according to the axis O_x (ωx)($\omega x = constant$).

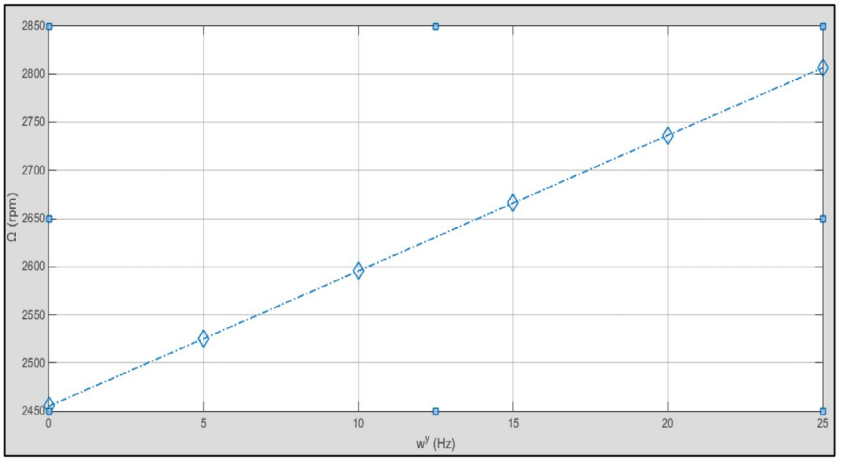

Figure 19. Speed of the intersection of the first direct mode with the right $f = \Omega/60$ with respect to rotation of the support according to the axis O_y (ωy)($\omega y = constant$).

4.2.6. Influence of the geometric shape of the rotary shaft:

To study the influence of the geometric shape of an on-board rotor, we used the same example taken above, we just changed the position of the disc and the bearings. The new system is shown in Figure 20 (rotor, free, bearings, bearings, and disc) (Figures 19 and 20).

In Figure 21 we can see the change in behaviour of on-board rotor.

Figure 22 shows the diagram of the first two frequencies for two rotations of the support ($\omega^x = 5, et\ 5$ Hz). Figure 23 shows the diagram of the first two frequencies for two rotations of the support ($\omega^y = 10, et\ 10$ Hz).

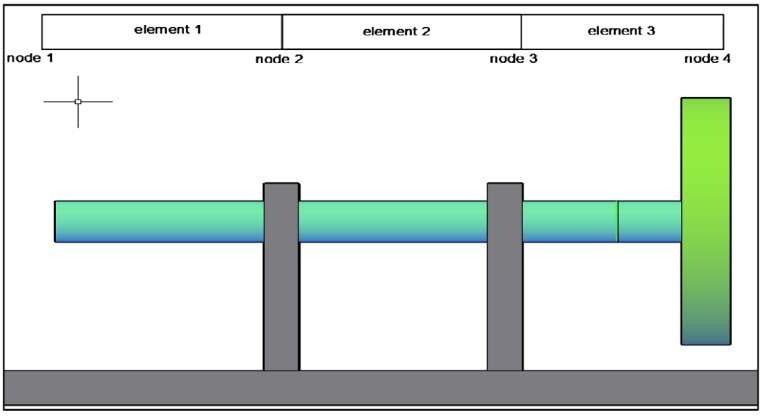

Figure 20. On-board rotor (Free, Bearings, Bearings, Disc).

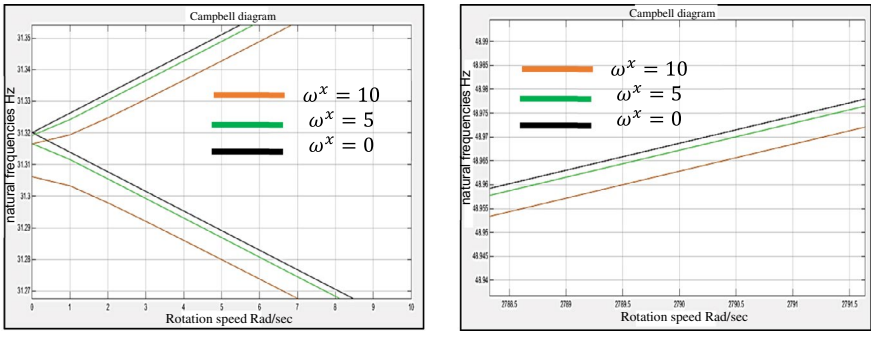

Figure 21. Campbell diagram of the first two frequencies $\omega^x = 0;5;10$ Hz.

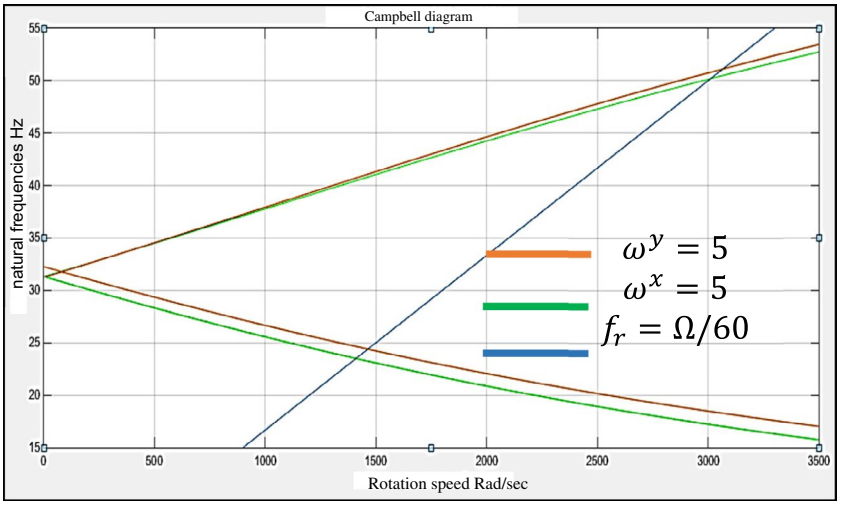

Figure 22. Campbell diagram of the first two frequencies $\omega^x = 5\ Hz$ and $\omega^y = 5\ Hz$.

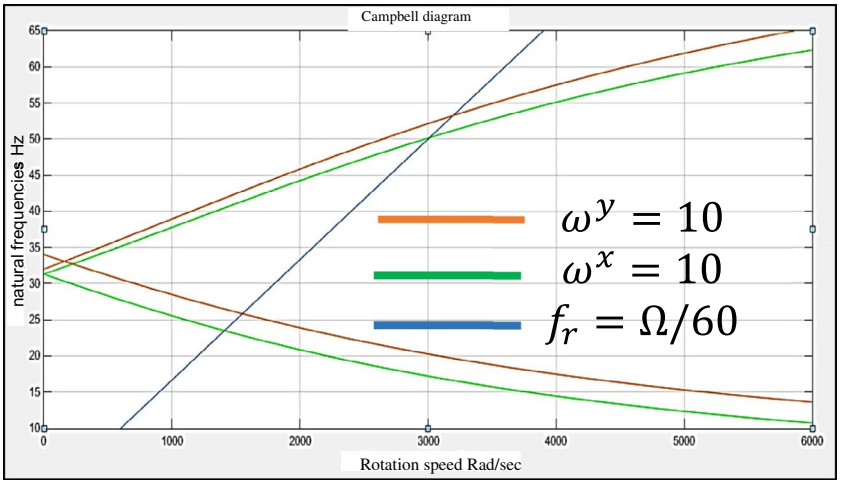

Figure 23. Campbell diagram of the first two frequencies ωx = *10 Hz*, $\omega^y = 10$ *Hz*.

5. Conclusion

The vibrational behaviour of on-board rotors analysis using the method of the hierarchical finite elements (p version of the MEF) with functions with Legendre polynomials form, combined with the standard method of finite elements (h version of the FEM) is treated in this paper (Figure 23).

The calculation of energy different components of the on-board rotor, the application of the method of Lagrange, and introducing features of the h-p version of the finite elements, has given us the equations of motion of the system. The calculation is done on an element, then after assembly will have the overall equation of the system.

A programme for calculating the natural frequencies and critical speeds was developed with MATLAB. The validation test programme shows the effectiveness of the method; convergence is achieved for a number of polynomials equal to seven, and the differences with the results obtained by other authors are very small (of the order of ten thousandth for the first frequency in the case of small disturbance around the axis O_x $\omega^x = 5$ Hz and a little more in the case $\omega^x = 10$ Hz).

Several examples are treated and this has allowed us to determine the influence of different geometric parameters of on-board rotor and also the influence of the movement of the support on the behaviour of the rotor.

This work has allowed us to reach the following conclusions:

- In the case of the use of the MEF h version convergence is obtained starting from the 6 elements, while in the case of the use of the p version, it is obtained starting from a polynomial degree p equal to 7. The calculation time is 02 s (Intel Cor2duo 2.5 GB, 2 GB RAM).
- The convergence of results can be controlled by increasing the polynomial degree (number of shape functions) and also the number of elements. The

difference in results between the two methods (h-p version and the classic version of h) is very small, but the benefit of h-p version is that you can control both parameters of the element (the polynomial degree and number of elements).

- We conclude that the convergences can be classified in a following way:
- h-version: convergence in an algebraic way.
- h-p version: convergence in an exponential way, or it can be improved by a suitable combination of the parameters (mesh degree h and polynomial degree p).
- The Legendre polynomial is used in this article, due to its very close approximation of the deformed shafts.
- The movement of the on-board rotor support amplifies the gyroscopic effect caused by the coupling of the displacements perpendicular to the axis of rotation, and creates an asymmetry in the movement of the rotor.
- In the case of disturbances in the neighbouring of the first critical speed, the influence of rotation of the support around the axis O_x (ω^x) is very low compared with the rotation of the support around the axis O_y (ω^y).
- From the results obtained in this work, we conclude that the rotation of the support around the axis parallel to the axis of rotation of the rotor has a great influence on the rigidity of the system and especially on the gyroscopic effect.
- The geometric parameters also have an influence on the vibration behaviour of on-board rotor. It is noted that it causes frequency variations and therefore variations in the critical speeds depending on the disc position.

Disclosure statement

No potential conflict of interest was reported by the authors.

ORCID

Ahmed Saimi http://orcid.org/0000-0002-3722-2526
Abdelhamid Hadjoui http://orcid.org/0000-0001-7216-8249

References

Babuska, I., & Guo, B. Q. 1992. The h, p and h-p version of the finite element method: Basis theory and applications. *Advances in Engineering Software, 15*, 159–174.

Babuška, I., & Suri, M. (1987). The h-p version of the finite element method with quasiuniform meshes. *RAIRO – Modélisation mathématique et analyse numérique, 21*, 199–238.

Banerjee, J. R. (2000). Free vibration of centrifugally stiffened uniform and tapered beams using the dynamic stiffness method. *Journal of Sound and Vibration, 233*, 857–875.

Bardell, N. S. (1996). An engineering application of the h-p version of the finite element method to the static analysis of a Euler-Bernoulli beam. *Computers & Structures, 59*, 195–211.

Bokaian, A. (1948). Natural frequencies of beams under compressive axial load. *Journal of Sound and Vibration, 126*, 49–65.

Boukhalfa, A., & Hadjoui, A. (2010). Free vibration analysis of an embarked rotating composite shaft using the h-p version of the FEM. *Latin American Journal of Solids and Structures, 7*(2).

Chen, L. W., & Ku, D. M. (1992). Dynamic stability of a cantilever shaft-disk system. *Journal of Vibration and Acoustics Transaction of the American Society of Mechanics Engineers, 114*, 326–329.

Chen, L. W., & Sheu, H. C. (1998). Stability behavior of a shaft-disk system subjected to longitudinal force. *Journal of Propulsion and Power, 14*, 375–383.

Choi II, S., Pierre, C., Ulsoy, A. G. (1995). Consistent modeling of rotating Timoshenko shaft subject to axial loads. *Journal of Sound and Vibration and Acoustics, 182*, 759–773.

Dakel, M. (2013). Steady-state dynamic behaviour of an on-board rotor under combined base motions. *Journal of Vibration and Control, 20*, 2254–2287. doi:10.1177/1077546313483791

Duchemin, M., Berlioz, A., & Ferraris, G. (2006). Dynamic behavior and stability of a rotor under base excitation. *Journal of Vibration and Acoustics, 128*, 576–585.

Eshienman, R. L., & Eubanks, R. A. (1967). On the critical speeds of a continuous shaft-disk system. *Journal of Engineering for Industry, 80*, 645–652.

Green, R. B. (1948). Gyroscopic effects on the critical speeds of flexible rotors. *Transaction of the American society of Mechanic Engineers, 70*, 309–376.

Heuveline, V., & Rannacher. 2003. Duality-based adaptively in h-p-finite element method. *Journal of Numerical Mathematics, 11*, 95–113. doi:10.1515/156939503766614126

Khader, N. (1995). Stability of rotating shafts loaded by follower axial force and torque load. *Journal of Sound and Vibration, 182*, 759–773.

Lalanne, M., & Ferraris, G. (1998). *Rotor dynamics prediction in engineering* (2nd ed.). Chichester: Wiley. 254 p.

Lin, S. C., & Hsiao, K. M. (2001). Vibration analysis of a rotating Timoshenko beam. *Journal of Sound and Vibration, 240*, 303–322.

Nelson, H. D., & McVaugh, J. M. (1976). The dynamics of rotor-bearing systems using finite elements. *ASME Journal of Engineering for Industry, 98*, 593–600.

Peano, A. (1976). Hierarchies of conforming finite elements for plane elasticity and plate bending. *Computers & Mathematics with Applications, 2*, 211–224.

Rao, S. S. (1983). *Rotor dynamics*. New York, NY: Wiley.

Szabo, B. (1985a). *A PROB theoretical manual release1*. St Louis, MO: Technologies Corp.

Szabo, B. (1985b). *A FIESTA theoretical manual release1*. St Louis, MO: Technologies Corp.